The Journal of Chemical Physics

RESEARCH ARTICLE | FEBRUARY 11 2015

The fundamental rotational interval of para-H_2^+ by MQDT-assisted Rydberg spectroscopy of H_2

Christa Haase; Maximilian Beyer; Christian Jungen; Frédéric Merkt

Check for updates

J. Chem. Phys. 142, 064310 (2015)
https://doi.org/10.1063/1.4907531

View Online
Export Citation

Articles You May Be Interested In

High-resolution spectroscopy and quantum-defect model for the *gerade* triplet *np* and *nf* Rydberg states of He_2

J. Chem. Phys. (February 2014)

High-resolution millimeter wave spectroscopy and multichannel quantum defect theory of the hyperfine structure in high Rydberg states of molecular hydrogen H 2

J. Chem. Phys. (December 2004)

Analysis of vibrational autoionization of CaF Rydberg states

J. Chem. Phys. (April 2019)

25 July 2026 17:53:19

AIP Advances
Why Publish With Us?
21DAYS average time to 1st decision
OVER 4 MILLION views in the last year
INCLUSIVE scope
Learn More
AIP Publishing

AIP Publishing

The fundamental rotational interval of para-H_2^+ by MQDT-assisted Rydberg spectroscopy of H_2

Christa Haase,[1] Maximilian Beyer,[1] Christian Jungen,[2,a)] and Frédéric Merkt[1]
[1]*Laboratorium für Physikalische Chemie, ETH Zürich, 8093 Zürich, Switzerland*
[2]*Laboratoire Aimé Cotton, CNRS, Université Paris-Sud 11, ENS-Cachan, Campus d'Orsay Bâtiment 505, 91405 Orsay, France*

(Received 18 December 2014; accepted 23 January 2015; published online 11 February 2015)

Transitions from selected *n*d Rydberg states of H_2 to n'p/f Rydberg series converging on the lowest two ($N^+ = 0$ and 2) rotational levels of the $X^+\,^2\Sigma_g^+$ ($v^+ = 0$) ground state of para-H_2^+ have been measured in the range 1-7.4 THz using a laser-based, pulsed, narrow-band source of submillimeter-wave radiation. The analysis of the spectra by multichannel quantum-defect theory (MQDT) has allowed a complete interpretation of the fine structures of the Rydberg series and their dependence on the principal quantum number. The extrapolation of the series to their limits with MQDT has enabled the determination of the first rotational interval of para-H_2^+, which is 174.236 71(7) cm^{-1} (5 223 485.1(2.3) MHz). © *2015 Author(s). All article content, except where otherwise noted, is licensed under a Creative Commons Attribution 3.0 Unported License.* [http://dx.doi.org/10.1063/1.4907531]

I. INTRODUCTION

Consisting of two protons and one electron, H_2^+ is the simplest stable molecule. It has two nuclear-spin isomers, para-H_2^+ and ortho-H_2^+, with singlet and triplet nuclear-spin functions, respectively. The energy-level structure of H_2^+ and of the deuterated isotopomers HD^+ and D_2^+ can be calculated with extreme accuracy by quantum-chemical methods.[1–6] The most recent calculations include relativistic corrections and quantum-electrodynamics corrections up to terms proportional to α^8,[5,6] where α is the fine-structure constant. For instance, the first vibrational intervals in H_2^+ and HD^+ (65 688 323.708 (2) MHz and 57 350 154.371 (2) MHz, respectively) were reported to be accurate to within 2 kHz. Other rovibrational intervals were calculated with uncertainties of at most 15 kHz for transitions involving vibrational levels below $v^+ = 8$. H_2^+, HD^+, and D_2^+ are thus the molecules with the most precisely known energy-level structure.

Paradoxically, H_2^+ is the molecular system that is most resistant to spectroscopic investigations. Not only does its positive charge prevent the generation of large concentrations in the gas phase, but, more importantly, the absence of a permanent electric dipole moment also implies that H_2^+ has neither a pure rotational nor a rovibrational spectrum in the electric-dipole approximation. Moreover, H_2^+ has mostly repulsive excited electronic states. Several of these excited states, such as the $1s\sigma_u$, the $2p\pi_u$, and the $3d\sigma_g$ states,[7–9] possess shallow minima at large internuclear distances, but their bound levels cannot be excited from low vibrational levels of the electronic ground state because of unfavorable Franck-Condon factors. Consequently, the low-lying rovibrational levels of the ground state of H_2^+ and D_2^+ are not observable by standard methods of optical spectroscopy.

The spectroscopic data available on the $X^+\,^2\Sigma_g^+$ state of H_2^+ (in the following, we designate the state labels and quantum numbers of the H_2^+ ion with a + superscript) were obtained in

(i) Studies by Carrington and his coworkers of the electronic spectrum of the A^+-X^+ transition, which lies in the microwave range of the electromagnetic spectrum and provides information on the highest vibrational levels of the X^+ state ($v^+ = 18$ and 19).[10]
(ii) Studies by Jefferts[11,12] of the magnetic-dipole spectrum connecting the different spin-rotation components of the $N^+ = 2$ rotational levels of the $X^+\,^2\Sigma_g^+$ ($v^+ = 4$–8) states of para-H_2^+ and the different hyperfine components of the $N^+ = 1$ rotational levels of the $v^+ = 4$–8 states of ortho-H_2^+. These studies provided the fine and hyperfine structure intervals but not the relative positions of the rovibrational levels.
(iii) Studies by Herzberg and Jungen[13] of the Rydberg spectrum of H_2, from which the positions of the ($v^+ = 0$–4, $N^+ = 0$–3) rovibrational levels of H_2^+ could be determined with a precision of about 0.2 cm^{-1}.
(iv) Sub-MHz-resolution studies of the hyperfine structure of the ($v^+ = 0, N^+ = 1$) level of ortho-H_2^+ [14,15] and of the $N^+ = 1$–$N^+ = 3$ rotational interval of ortho-H_2^+ [16] by millimeter-wave spectroscopy of Rydberg-Rydberg transitions.
(v) Studies of the photoelectron spectrum of H_2, starting with the work of Åsbrink,[17] who was the first to partially resolve the rotational structure by recording a Ne I photoelectron spectrum (resolution in the range 40–80 cm^{-1}). Later measurements by pulsed-field-ionization zero-kinetic-energy photoelectron spectroscopy enabled a

[a)]Also at Department of Physics and Astronomy, University College London, London WC1E 6BT, United Kingdom.

25 July 2026 17:53:19

 © Author(s) 2015

higher resolution, down to about 1 cm^{-1},[18] and the determination of almost all bound vibrational levels of H_2^+.[19]

Measurements of the $(v^+ = 0, N^+ = 0)$ to $(v^+ = 4, N^+ = 1)$ and the $(v^+ = 0, N^+ = 0)$ to $(v^+ = 0, N^+ = 1)$ transitions of HD^+, which has a small permanent electric dipole moment and thus weak pure rotational and vibrational spectra, have also been reported.[20,21] The frequency of the $(v^+ = 0, N^+ = 0)$ to $(v^+ = 1, N^+ = 1)$ transition was determined to be 58 605 052.000(64) MHz [21] and found to deviate by 2.6 σ from the calculated value (58 605 052.156 (2) MHz),[5] a discrepancy attributed to unknown systematic errors. The $N^+ = 0$ to $N^+ = 1$ pure rotational transition in HD^+ was detected,[20] but its frequency was not given.

We report here on the first experimental determination of the $N^+ = 0$–$N^+ = 2$ rotational interval of the $X^+\,^2\Sigma_g^+$ $(v^+ = 0)$ ground state of H_2^+ by THz spectroscopy of Rydberg-Rydberg transitions of H_2. To designate the Rydberg states of para-H_2 converging to the rotational levels of the ground vibronic state of H_2^+, we use the notation $n\ell N^+_N$, where n, ℓ, N^+, and N represent the principal and orbital angular momentum quantum numbers of the Rydberg electron, the H_2^+ rotational angular momentum quantum number, and the quantum number for the total angular momentum excluding spins, respectively. The principle of the determination is illustrated in Fig. 1 and involves the extrapolation of non-penetrating nf Rydberg series converging on the $N^+ = 0$ and $N^+ = 2$ levels of the ion, accessed from two different initial states, the $40d0_2$ and $20d2_1$ Rydberg states. nd-nf Rydberg-Rydberg transitions involving a change in the ion-core rotational quantum number are extremely weak. To overcome this problem, we have recorded spectra from two different initial Rydberg levels, one with an $N^+ = 0$ ion core to access the $nf0_3$ Rydberg series converging to the $N^+ = 0$ ionization limit, the other with an $N^+ = 2$ ion core to access $nf2_{1,2}$ Rydberg series converging to the $N^+ = 2$ ionization limit. The spacing between the $20d2_1$ and $40d0_2$ initial states needed to determine the positions of all levels on the same energy scale was extracted from measurements of transitions from both of these states to the same set of npN^+_1 $(N^+ = 0, 2)$ states with mixed $N^+ = 0$ and $N^+ = 2$ ion-core character. This was achieved by exploiting the rotational channel interaction depicted by the double-sided red arrow in Fig. 1. The relative positions of all Rydberg levels connected by the transitions were then used to extrapolate the series to $N^+ = 0$ and 2 series limits using multichannel quantum-defect theory (MQDT), and the set of energy- and internuclear-distance-dependent quantum-defect functions reported in Ref. 22, which were shown in previous work to enable an accuracy in the extrapolation of better than 500 kHz.[14,22,23] For the measurements, which required a narrow-band source of submillimeter-wave radiation tunable between 0.4 and 7.5 THz, we used a home-built laser-based source of THz radiation described in Refs. 24 and 25.

II. EXPERIMENTAL PROCEDURE

The experiments were carried out using the resonant three-photon excitation sequence

$$\begin{aligned} np, f[N^+ = 0, 2]_N &\xleftarrow{\text{THz}} n'd[N^+ = 0, 2]_{N'} \\ &\xleftarrow{\text{UV}} B\,^1\Sigma_u^+(v = 4, N = 1) \\ &\xleftarrow{\text{VUV}} X\,^1\Sigma_g^+(v = 0, N = 0) \end{aligned} \quad (1)$$

depicted schematically in Fig. 2(b). The vacuum-ultraviolet (VUV) radiation near λ = 105 nm needed to excite molecular hydrogen from the $X\,^1\Sigma_g\,(v = 0, N = 0)$ ground state to the $B\,^1\Sigma_u^+(v = 4, N = 1)$ state was generated by resonance-enhanced sum-frequency mixing $(\nu_{VUV} = 2\nu_{UV} + \nu_{VIS})$ in xenon, making use of the $(5p)^5\,(^2P_{3/2})\,6p[1/2]_0 \leftarrow (5p)^6\,^1S_0$ two-photon resonance of Xe at a wave number $2\tilde{\nu}_{UV}$ = 80 118.9839 cm^{-1}. The UV and visible (VIS) laser beams used for sum-frequency mixing were generated by two Nd:YAG pumped, pulsed dye lasers, one of which was frequency-doubled to generate $\lambda_{UV} \sim 250$ nm for the two-photon resonance. The UV laser radiation in the range

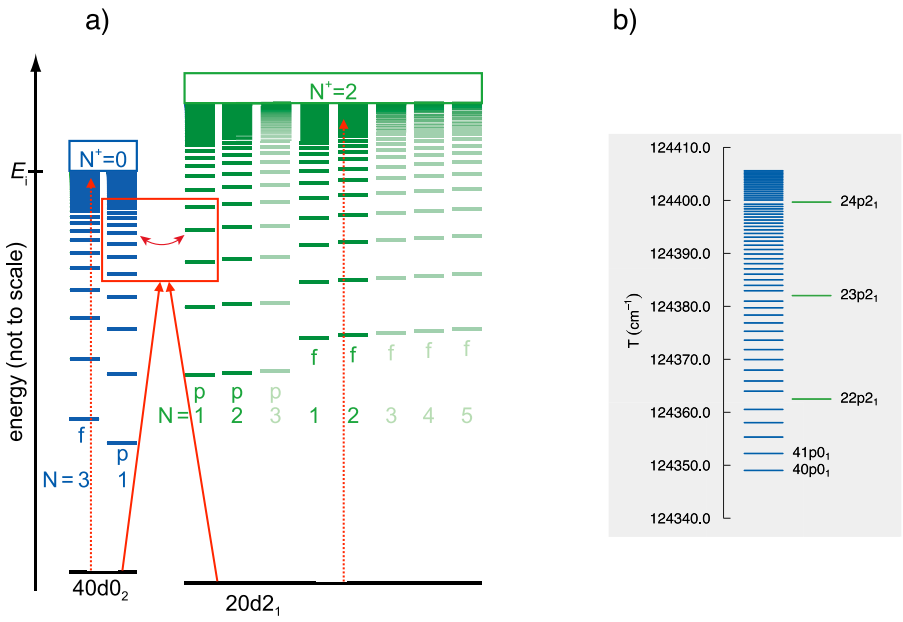


FIG. 1. (a) Energy-level diagram of the np and f Rydberg series of H_2 converging on the $N^+ = 0$ and 2 rotational levels of the $X^+\,^2\Sigma_g^+(v^+ = 0)$ ground state of H_2^+. The dashed arrows designate transitions to the $nf0_3$ and $nf2_2$ Rydberg series used in the Rydberg series extrapolation, and the full arrows the transitions to the $np0,2_1$ Rydberg states of mixed ion-core rotational character used to determine the relative positions of the two initial Rydberg levels ($40d0_2$ and $20d2_1$). Optically accessible series are drawn in bright color. (b) Enlarged view of the interacting $np0,2_1$ series in the region highlighted by a frame in panel (a).

25 July 2026 17:53:19

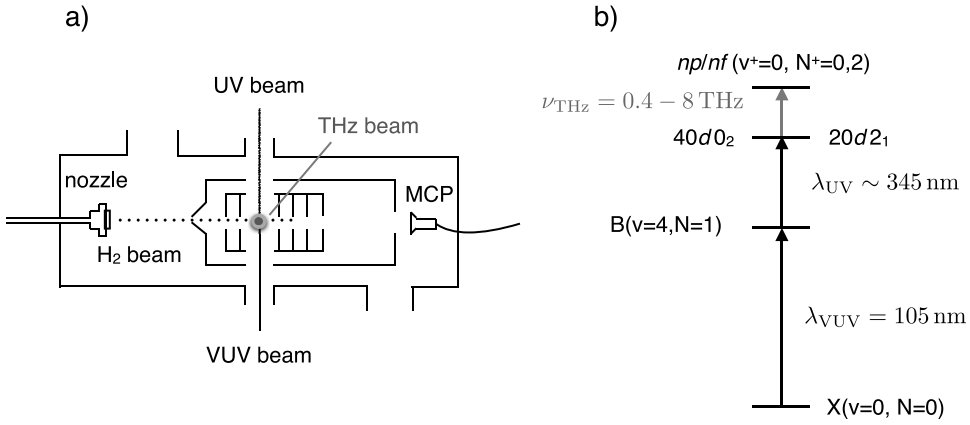


FIG. 2. (a) Schematic representation of the experimental configuration. (b) Excitation sequence used to access Rydberg series converging on either of the two lowest-lying rotational levels of para-H_2^+ ($X^+\,^2\Sigma_g^+(v^+=0)$).

between 340 and 348 nm used to induce transitions from the $B(v=4, N=1)$ state to the $40d0_2$ and $20d2_1$ initial Rydberg states was produced by doubling the frequency of a third pulsed dye laser pumped by the same Nd:YAG laser. Radiation tunable between 0.4 and 8 THz was then employed to induce transitions from the selected initial Rydberg levels ($40d0_2$ or $20d2_1$) to the final $np0_1$, $nf0_3$, $np2_1$, and $nf2_2$ Rydberg states (see Fig. 1). Pulsed, tunable THz radiation was generated by difference-frequency mixing of the near-infrared (NIR) pulse-amplified outputs of two narrowband, Nd:YVO_4-pumped titanium-sapphire (Ti:Sa) ring lasers in a crystal of the organic material called DAST (see Refs. 24 and 25 for details). The cw outputs of these Ti:Sa ring lasers were converted into pulses by two acousto-optic modulators and then pulse-amplified in Nd:YAG pumped Ti:Sa crystals using a multipass bow-tie configuration to generate NIR pulses with energies of ∼8 mJ and THz pulse energies of about ∼15 nJ. NIR pulse lengths were typically set to ∼40 ns, corresponding to a Fourier-transform-limited bandwidth of ∼15 MHz. Tunable THz radiation was generated by fixing the frequency of the first and scanning the frequency of the second NIR ring laser. The absolute frequency of both NIR lasers was determined by Doppler-free saturation spectroscopy of I_2, and the relative frequency calibration was performed by recording the transmission spectrum through a confocal Fabry-Pérot etalon (FSR = 149.963(3) MHz, finesse = 30) that was length-stabilized using a HeNe laser.[25] The frequency of the first ring laser was actively stabilized to a transmission maximum of the same Fabry-Pérot etalon, which resulted in an accuracy of 2.8 MHz for the THz radiation frequency, as described in Ref. 25. The THz excitation pulses were applied 20 ns after the VUV and UV laser pulses, which were overlapped temporally because of the short lifetime of the $B(v=4, N=1)$ state. The experimental cycles were triggered at a repetition rate of 25 Hz.

The vacuum chamber in which the experiments were performed is displayed schematically in Fig. 2(a). A supersonic beam of H_2 molecules was generated by expansion of pure H_2 into vacuum through the orifice of a pulsed nozzle that was operated at a stagnation pressure of ∼3 bars. The innermost part of the beam was selected with a skimmer to reduce the Doppler width. The THz, VUV, and UV radiation beams intersected the supersonic beam at right angles on the axis of a set of resistively coupled metallic extraction plates that were used for the selective field ionization of the final Rydberg states and to accelerate the generated H_2^+ ions towards a microchannel-plate (MCP) detector located at the end of a short time-of-flight tube. The photoexcitation region and the time-of-flight tube were surrounded by two concentric mumetal shields to suppress stray magnetic fields. Stray electric fields in the excitation region were reduced to less than 1 mV/cm by applying small compensation fields along the symmetry axis of the electrode stack, as described in Ref. 26.

The final Rydberg states were ionized selectively using a sequence of two pulses applied about 400 ns after the laser pulses. The first pulse had an electric field strength of 13.2 V/cm and the second pulse a strength in the range 79–132 V/cm, depending on the principal quantum number of the final Rydberg state. The first pulse separated prompt ions from ions generated by the selective-field-ionization pulse. Spectra of Rydberg states located below the $N^+ = 0$ ionization threshold were obtained by monitoring the H_2^+ signal generated by the second electric field pulse at the MCP detector as a function of the frequency of the THz radiation. Spectra of the autoionizing Rydberg states converging to the $N^+ = 2$ threshold were measured by recording the H_2^+ ions produced by autoionization and extracted by the first pulse.

III. EXPERIMENTAL RESULTS

Spectra of the $np0_1$ and $nf0_3$ Rydberg series of H_2 in the range n = 48–64 recorded from the $40d0_2$ intermediate level are displayed in Fig. 3. Whereas the $nf0_3$ series is regular in this range of n values, the $np0_1$ series is strongly perturbed by the $np2_1$ series. The perturbation can be recognized by the evolution with n of the spacing between the $np0_1$ and $nf0_3$ levels, which is positive at n = 48, then gradually decreases and becomes negative above n = 50, reaches a minimum at n = 55 just below the position of the $23p2_1$ perturbing level, above which it abruptly becomes positive (at n = 57) and starts decreasing again. Near the $23p2_1$ perturbing level, the perturbation strongly reduces the $N^+ = 0$ character of the states, which prevented the observation of the $56p0_1$ level. This behavior is characteristic of rotational channel interactions[13,27] and can be quantitatively modeled by MQDT calculations (described in Sec. IV), as illustrated in Fig. 4

25 July 2026 17:53:19

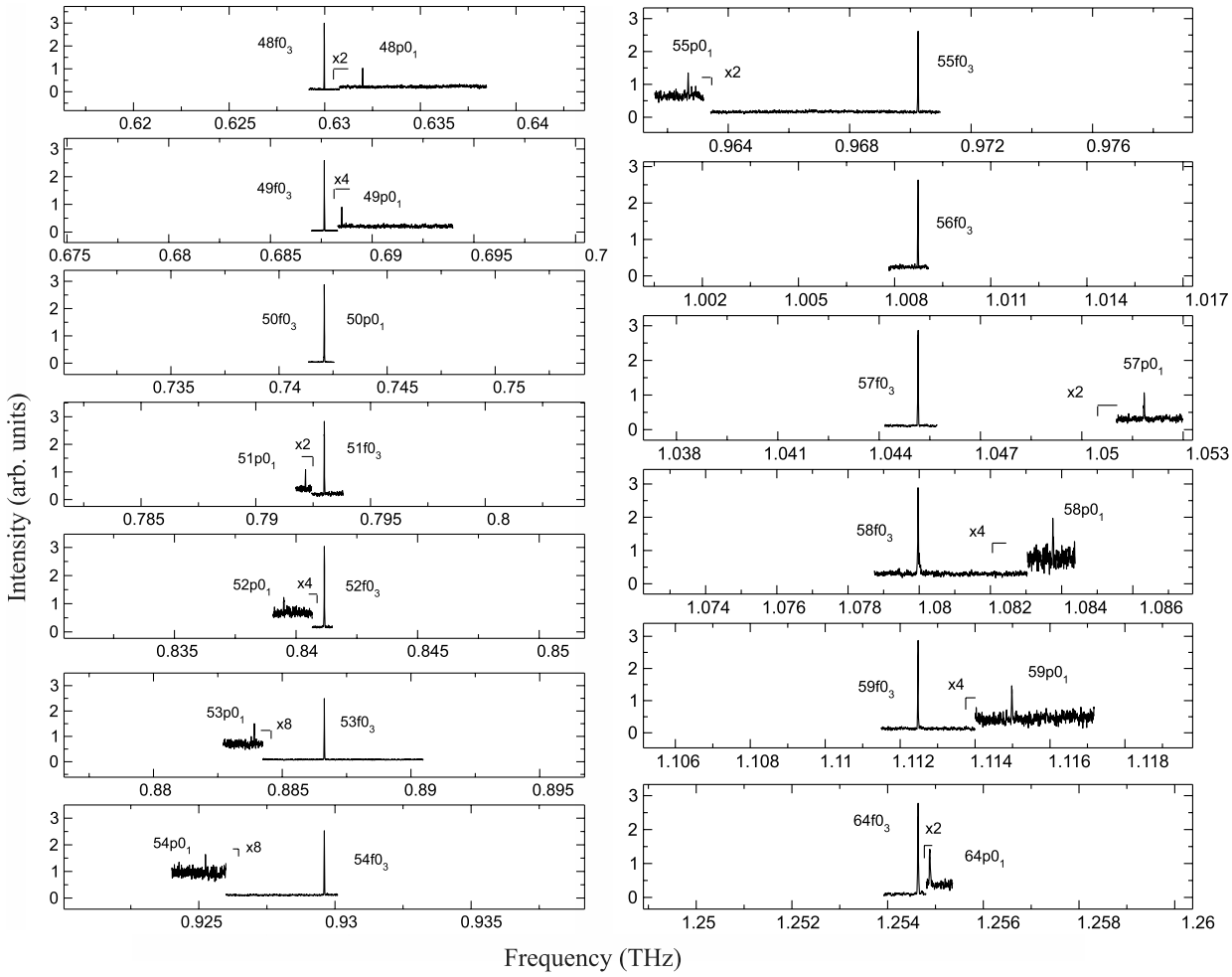


FIG. 3. Spectra of transitions from the 40d0$_2$ state to nf0$_3$ and np0$_1$ Rydberg states with n in the range 48-64. In each spectrum, the transition to the unperturbed nf0$_3$ state has been placed at the center of the frequency scale so that the perturbations of the np0$_1$ series are easily recognizable.

by the comparison between calculated (open circles) and measured (crosses) effective quantum defects $\mu_{\rm eff}$ (determined from the spectral positions using Rydberg's formula $\tilde{\nu} = E_{\rm I}/(hc) - R_{\rm H_2}/(n-\mu_{\rm eff})^2$, where $E_{\rm I}$ is the ionization energy from the selected intermediate state).

Fig. 4 reveals that the perturbations of the np0$_1$ series are modulated by the successive members of the np2$_1$ series. Near the 23p2$_1$ perturbing level, the np0$_1$ levels gain $N^+ = 2$ character, which renders them observable not only from the 40d0$_2$ level but also from the 20d2$_1$ level. Measurements of transitions to the 54, 55, 57, and 58p0$_1$ levels from the 40d0$_2$ and the 20d2$_1$ levels enabled us to determine the spacing between these two levels to be 0.979 862 45(59) THz, and thus to derive a common relative energy scale for f levels converging on the $N^+ = 0$ and 2 limits, which is a prerequisite for the determination of the $N^+ = 0$–$N^+ = 2$ interval of the $X^+\,^2\Sigma_g$ ($v^+ = 0$) ground state of H_2^+.

Spectra of transitions from the 20d2$_1$ intermediate level to nf2$_N$ Rydberg states of selected n value between 30 and 70 are presented in Fig. 5. Because the 20d2$_1$ level has pure singlet (i.e., $S = 0$, $N = 1$, $J = 1$) character, the dominant transitions in these spectra are those to singlet nf2$_{N=J}$ levels, which appear as sharp lines with laser-limited bandwidths up to $n = 60$ and then broaden slightly because of the gradual evolution of the fine structure of the nf levels, as will be discussed in more detail in Sec. IV. The dominant Rydberg-Rydberg transitions follow the propensity rules $\Delta S = 0$ and $\Delta N = \Delta\ell$,[14] which strongly favor the singlet nf2$_{N=2,J=2}$ series.

Beyond $n = 45$, weak satellite lines appear around the strong transitions to the nf2$_2$ levels. These weak lines originate from the fact that the exchange term of the electron-electron Coulomb interaction between the Rydberg and core electrons scales as n^{-3}, whereas the spin-rotation interaction of the $N^+ = 2$ ion-core level is independent of n. Consequently, as n increases, the core-electron spin gradually decouples from the Rydberg-electron spin and recouples to the core rotation. A mixing of singlet and triplet character results, which makes the triplet ($S = 1$) levels of the nf2$_1$ and nf2$_3$ states with $J = 2$ character weakly observable from the 20d2$_1$ initial level. Indeed, only the $J = 2$ components of the nf2$_1$ and nf2$_3$ triplet states can mix with, and gain intensity from, the strong nf2$_{N=2,J=2}$ series. No mixing between $S = 0$ and $S = 1$ channels can occur in the $N^+ = 0$ series because the spin-rotation interaction in the ion core vanishes when $N^+ = 0$. In the Rydberg states of ortho-H_2, the primary source of mixing between $S = 0$ and $S = 1$ channels is the hyperfine interaction in the ion core, as discussed in detail in Ref. 14.

25 July 2026 17:53:19

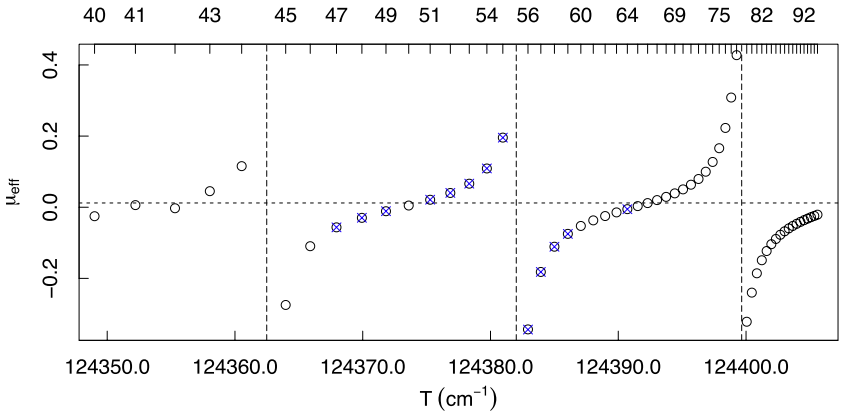


FIG. 4. Evolution of the effective quantum defect μ_{eff} of the np0$_1$ Rydberg series as a function of the principal quantum number n (top horizontal axis) and the term value T above the rovibronic ground state of H_2. The dashed, vertical lines represent the positions of the np2$_1$ perturbers. Calculated values are marked as black circles, experimental values as blue crosses.

The positions of all levels for which an accurate calibration could be performed are listed in Table I relative to the position of the 20d2$_1$ level. Because the splitting of the nf2$_2$ levels could only be observed as a broadening of the lines, the positions of these levels given in the table correspond to the center of gravity of the intensity distribution. The experimental uncertainties of most levels are in the range between 3 and 6 MHz and correspond roughly to a fifth of the full-width at half-maximum of the observed transitions. They resulted primarily from the statistical uncertainties arising from the determination of the line centers and the frequency calibration procedure.

The following sources of systematic errors were also considered:

(i) DC Stark shifts by residual electric fields
Our measurement procedure involved compensating stray electric fields to below 1 mV/cm. From measurements of the Stark effect in d → f transitions between n = 40 and 51, and by exploiting the n^7 scaling of the polarizability, we estimate the maximal shift for the transitions to all measured f levels to be 100 kHz.

(ii) Pressure shift
The pressure shift in high Rydberg states arises primarily from the scattering of the Rydberg electron with neutral atoms and molecules located within the Rydberg-electron orbit.[28] Because the shift is approximately the same for the initial and final states of the measured transitions, its effect on the transition frequen-

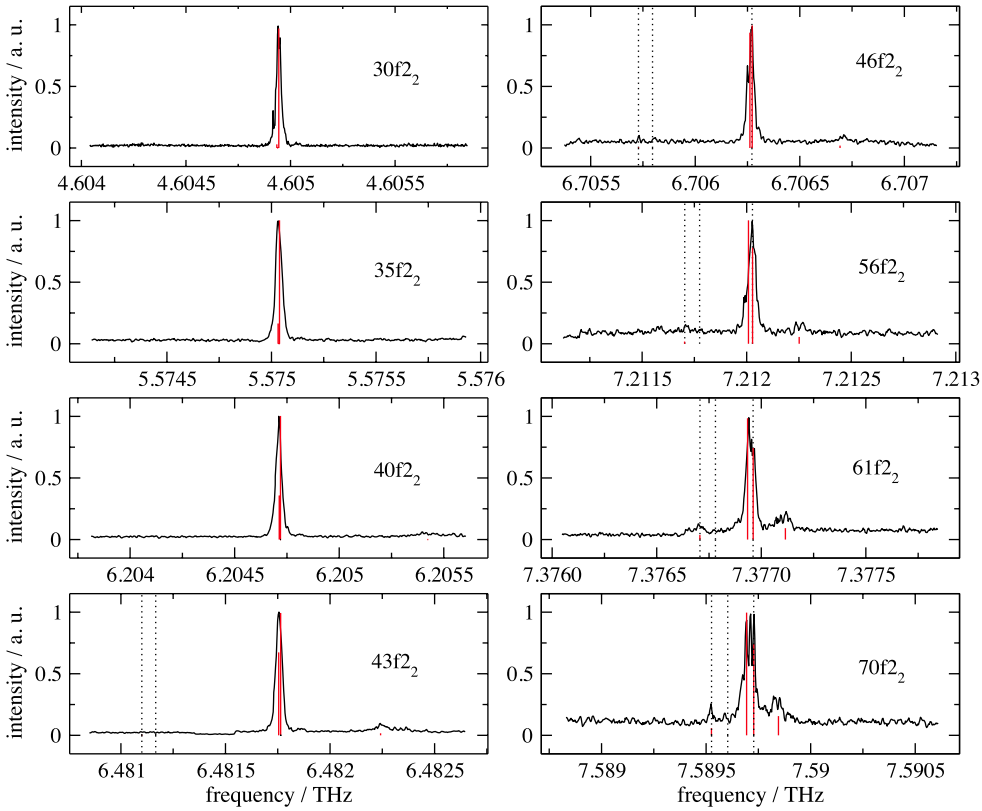


FIG. 5. Spectra of transitions from the 20d2$_1$ state to nf2$_2$ Rydberg states of para-H_2. In each spectrum, the dominant line corresponds to transitions to the singlet nf2$_2$ levels. The weak transitions, indicated by dashed and dotted vertical lines, on the low- and high-frequency sides of these dominant lines correspond to transitions to the $J = 2$ components of nf2$_1$ triplet levels, which gain intensity at high n values because of the mixing of singlet and triplet character induced by spin-rotation interaction in the ion-core $N^+ = 2$ level.

25 July 2026 17:53:19

TABLE I. Experimental positions of the Rydberg states of para-H_2 belonging to series converging to the $N^+ = 0$ and 2 rotational levels of the $X^{+2}\Sigma_g^+(v^+ = 0)$ ground state of H_2^+ relative to the position of the $20d2_1$ level and comparison with the results of MQDT calculations. The experimental uncertainties given in parentheses are statistical uncertainties (1σ), resulting from the determination of the line centers and the frequency-calibration procedure.

Level	E_{exp}/h (THz)	$(E_{exp} - E_{calc})/h$ (MHz)
$20d2_1$	0.000 000 0(13)	...
$40d0_2$	0.979 862 45(57)	...
$45f0_3$	1.412 939 7(31)	7.9
$46f0_3$	1.483 155 2(31)	−1.5
$47f0_3$	1.548 464 0(31)	8.5
$48f0_3$	1.609 837 6(31)	8.4
$49f0_3$	1.667 510 0(32)	7.6
$51f0_3$	1.772 848 5(34)	−0.3
$52f0_3$	1.821 025 0(32)	0.9
$53f0_3$	1.866 497 5(31)	−0.4
$54f0_3$	1.909 472 3(15)	4.9
$55f0_3$	1.950 114 4(31)	2.0
$56f0_3$	1.988 593 3(32)	2.3
$57f0_3$	2.025 014 4(33)	−2.2
$58f0_3$	2.059 830 7(36)	−7.9
$59f0_3$	2.092 635 6(33)	6.1
$64f0_3$	2.234 498 1(34)	3.8
$69f0_3$	2.346 671 4(38)	2.9
$74f0_3$	2.436 879 5(36)	2.0
$78f0_3$	2.496 902 4(47)	−5.6
$79f0_3$	2.510 503 8(40)	−3.9
$80f0_3$	2.523 594 6(61)	0.4
$47p0_1$	1.552 261 0(31)	−3.0
$48p0_1$	1.611 844 4(31)	−5.9
$49p0_1$	1.668 371 4(31)	−5.2
$51p0_1$	1.772 028 4(38)	−9.4
$52p0_1$	1.819 358 6(41)	−11.3
$53p0_1$	1.863 778 4(33)	−5.2
$54p0_1$	1.905 106 6(26)	−5.7
$55p0_1$	1.942 543 3(31)	4.4
$57p0_1$	2.031 709 4(27)	−0.4
$58p0_1$	2.063 620 6(28)	4.0
$59p0_1$	2.095 141 0(32)	2.5
$64p0_1$	2.234 745 4(34)	1.0
$35f2_2$	5.575 034 7(38)	7.0
$40f2_2$	6.204 710 9(52)	−7.7
$43f2_2$	6.481 758 0(39)	−4.2
$44f2_2$	6.561 700 6(57)	−1.3
$46f2_2$	6.706 267 0(40)	−1.4
$56f2_2$	7.212 021 7(36)	3.4
$61f2_2$	7.376 947 5(37)	4.4
$44f2_3(J = 2)$	6.562 189 5(63)	...
$46f2_3(J = 2)$	6.706 709 1(51)	...
$56f2_3(J = 2)$	7.212 255 8(58)	...
$61f2_3(J = 2)$	7.377 106 8(55)	...
$61f2_1(J = 2)$	7.376 700 9(55)	...

cies is expected to be negligible (see also discussion in Ref. 14).

(iii) AC Stark shift
An AC Stark shift would lead to a shift of the transition frequencies that is dependent on the intensity of the THz radiation. To determine a possible shift, measurements of the $54f0_3 \leftarrow 40d0_2$ transition were performed at several intensities of the NIR (and thus THz) radiation. No shift in the transition frequency was observed within the accuracy of the measurements (~2.8 MHz, see Ref. 25).

(iv) Doppler shifts
Such shifts can be estimated from the velocity component of the supersonic beam along the propagation axis of the THz radiation according to $\nu = \nu_0(1 + v/c)$. Because the supersonic beam propagates perpendicularly to the THz-radiation beam and the geometric constraints of the experiment limit a possible deviation from a perpendicular arrangement to less than 0.5°, we estimate from the H_2 beam velocity of 2 500 m/s that a possible Doppler shift could not exceed 2 MHz at the highest frequencies (7 THz) and 300 kHz at 1 THz.

Because these sources of systematic errors appear independent, we estimate that the overall systematic uncertainty of the frequencies reported in Table I is about 2 MHz and does not make a significant contribution to the overall uncertainty.

IV. MQDT CALCULATIONS AND DETERMINATION OF THE FUNDAMENTAL ROTATIONAL INTERVAL IN PARA-H_2^+

When extrapolating the Rydberg series to their limit, it is necessary to consider the fine structure of the Rydberg states and their evolution with the principal quantum number. In the case of para-H_2, which does not have a hyperfine structure, the fine structure originates from: (i) the exchange term of the electrostatic interaction between the Rydberg and the core electron, which couples the two electron spins and results in a splitting between singlet and triplet levels, (ii) the effects of core penetration by the Rydberg electron and of the long-range interaction between the multipole moments of the ion core and the Rydberg electron (penetration effects are dominant in the p series, whereas the members of the f series are mostly affected by long-range interactions[29] but both interactions contribute to the quantum defects), (iii) the spin-orbit interaction of the Rydberg electron, and (iv) the spin-rotation interaction in the $N^+ = 2$ ion core, which splits the $N^+ = 2$ level into two states with $J^+ = 3/2$ and 5/2 separated by 105.4 MHz.[4,5] The interactions (i)-(iii) contribute to the quantum defect and scale as n^{-3}, whereas interaction (iv) is a core property and therefore does not depend on n. Consequently, at very high n values, the dominant fine-structure interval is the 105.4 MHz spin-rotation splitting of the $N^+ = 2$ ion-core rotational level. In this case, the two electron spins are decoupled, and the Rydberg states are of mixed singlet and triplet character. In contrast, the spin-rotation interaction of the core is not observable for the $23p2_1$ and $20d2_1$ levels because it is much weaker at these low n values than interactions (i) and (ii), which entirely quench it. Singlet-triplet mixing does not occur in the series converging on the $N^+ = 0$ level, which is not affected by the spin-rotation interaction, as explained above.

In the range of n values of the levels under investigation, which were restricted to the region $n \leq 70$ to avoid systematic errors from the Stark shifts induced by residual stray fields, the energy level structure evolves from a situation governed by the interaction hierarchy (ii) > (i) ≫ (iv) > (iii) at $n = 30$, where S

25 July 2026 17:53:19

is a good quantum number, to one governed by the hierarchy (ii) > (iv) ≥ (i) > (iii) at $n = 70$, where the effects of singlet-triplet mixing and N mixing become observable (see Fig. 5 and the discussion in Sec. III). The evolution of the fine structure with n is correctly described by including all relevant angular momenta in the frame transformation upon which the MQDT treatment relies, as explained in Refs. 14 and 22. This evolution is depicted in Fig. 6(a), which shows the results of model MQDT calculations restricted to $v^+ = 0$ ionization channels to avoid perturbations of the level structure from vibrational channel interactions. The $J = 1$ (red) and $J = 2$ (blue) fine-structure components of the $nf2_{N=1-3}$ levels with n values in the range 30 to 150 are plotted with respect to the center of gravity ($\nu_{\mathrm{cog},\,N=2}$) of the $N = 2$ manifold at the corresponding n value. The grey dashed horizontal lines correspond to the n values for which measurements were carried out (see Fig. 5). Because of the strength and the n^{-3} dependence of interaction (ii), only the $N = 2$ levels are located in the frequency range covered by the figure below $n = 50$. Beyond $n = 50$, the $S = 1, J = 2$ component of the $nf2_3$ level and the $S = 1, J = 1,2$ components of the $nf2_1$ level enter the range of the figure from the right and the left, respectively, and the level structure rapidly evolves, at increasing n values, into two groups of levels separated by the spin-rotational interval of the $N^+ = 2$ state of H_2^+. Several perturbations of the level structure by rotational channel interactions are observed below $n = 70$, the most prominent of which is apparent around $n = 63$ and results from interactions with the $16f4_{1,2}$ levels.

The positions of the $J = 2$ levels in Fig. 6(a) closely match the fine structure observed in Fig. 5. The resolution of the experiment did not allow us to observe the three components of the central $N = 2$ manifold other than through a line broadening beyond $n = 60$, which originates from the increasing spacing between the two $J = 2$ components. The weak satellite lines observed in the experimental spectra beyond $n = 43$ exactly correspond to the positions calculated for the $nf2_3(S = 1, J = 2)$ and $nf2_1(S = 1, J = 2)$ levels. Calculations including all vibrational channels up to $v^+ = 10$ did not significantly modify the relative positions of the fine-structure components compared to that displayed in Fig. 6(a) but shifted their center of gravity by several tens of MHz in the vicinity of the $n = 42$ levels as a result of a perturbation caused by the $7f2_2(v^+ = 1)$ level. A comparison of the fine structures calculated for the central $N = 2$ manifold with (thick lines) and without (thin lines) consideration of the vibrational channel interactions is presented on an expanded

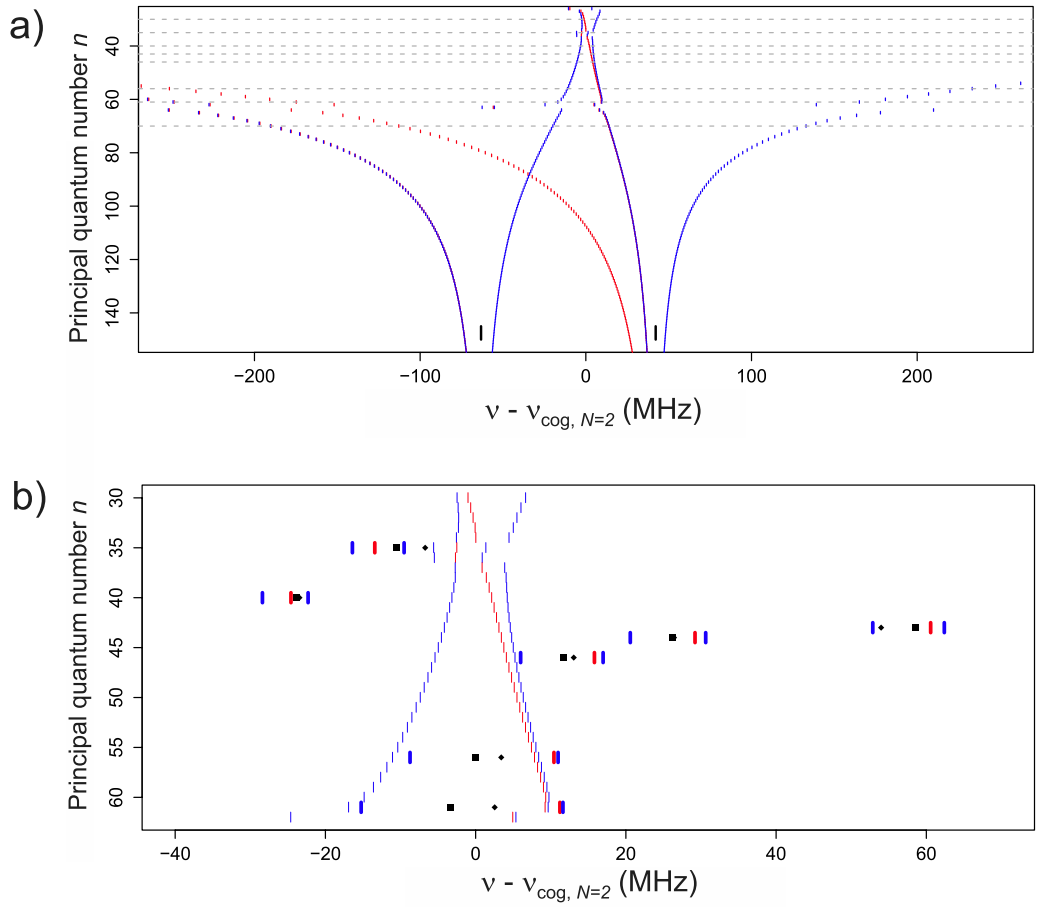


FIG. 6. (a) Positions, with respect to the center of gravity ($\nu_{\mathrm{cog},\,N=2}$) of the $N = 2$ manifold, of the $nf2_{N=1-3}$ Rydberg states with $J = 1$ (red) and 2 (blue) belonging to series converging on the two spin-rotational components, indicated by bold short vertical bars, of the $N^+ = 2$ rotational level of H_2^+. The dashed horizontal lines indicate the n values for which measurements were performed. (b) Comparison of the central $nf2_2$ levels with $J = 1$ (red) and 2 (blue) calculated with (thick lines) and without (thin lines) consideration of the vibrational channel interactions. The full squares mark the position of the center of gravity obtained by weighting the levels with their singlet character, and the diamonds correspond to the results of the MQDT calculations carried out by including only $S = 0$ ionization channels and neglecting the spin-rotational splitting of the $N^+ = 2$ level.

25 July 2026 17:53:19

scale in Fig. 6(b). The full squares mark the position of the center of gravity, obtained by weighting the levels with their singlet character, and the diamonds correspond to the results of a MQDT calculation carried out by including only $S = 0$ ionization channels and neglecting the spin-rotational splitting of the $N^+ = 2$ level. The positions of the diamonds and squares agree within 5 MHz for the $nf2_2$ levels studied experimentally. This excellent agreement *implies* that the position of the "pure" $N^+ = 2$ rotational level (i.e., its position relative to that of the $20d2_1$ level, neglecting the spin-rotation interaction) can be determined by extrapolating the centers of gravity of the $nf2_2$ lines observed experimentally (see Fig. 5 and Table I) in a MQDT fit which includes all relevant vibrational ionization channels up $v^+ = 10$ but neglects the $S = 1$ channels and the spin-rotational splitting of the $N^+ = 2$ level.

The pure rotational interval between the $N^+ = 0$ and $N^+ = 2$ levels and the energy of the $20d2_1$ level with respect to the $N^+ = 0$ ionization threshold of H_2 were determined from the experimental data by MQDT to be 174.236 71(7) cm^{-1} (or 5 223 485.1(2.3) MHz) and $E(20d2_1)/(hc) = -101.322\,62\,(9)$ cm^{-1}, respectively, in a least-squares fit of these two intervals using all 39 $np0_1$, $nf0_3$, and $nf2_2$ transition frequencies listed in Table I. The fit did not involve adjustment of any of the quantum defect parameters, which are known accurately,[22] and resulted in a dimensionless root-mean-square deviation of 1.23 and residuals that all lie within 11.3 MHz of the experimental values. Our value of the first rotational interval in para-H_2^+ represents the most accurate experimental value of this quantity obtained so far.

The experimental data were acquired in an n range where the effects of the spin-rotation interaction in the ion core are only weakly noticeable, primarily through the intensity, rather than the positions, of the satellite lines observed in Fig. 5. This implies that the fine-structure of the observed spectra does not enable a precise determination of the spin-rotation splitting of the $N^+ = 2$ rotational level. Exploratory calculations indicate that measurements at $n = 100$ and beyond would be necessary for this purpose. Such measurements, in autoionizing series, are complicated by the inhomogeneous fields generated by the ions released in the autoionization process.

V. CONCLUSIONS

The rotational interval between the $N^+ = 0$ and $N^+ = 2$ levels of the ground vibronic state of H_2^+ has been determined to be 174.236 71(7) cm^{-1} (5 223 485.1(2.3) MHz) from measurements of transitions between selected nd and np and nf Rydberg states of para-H_2 belonging to series converging to the lowest two rotational levels of para-H_2^+ and extrapolation of the series to their limits using MQDT. This value is in agreement, within the experimental uncertainty, with the more precise theoretical value of 174.236 742 482 4 cm^{-1}.[4,5]

The evolution of the fine structure of the $nf2_2$ Rydberg series for increasing n values has been studied from a situation where the levels can be labeled by the total electron-spin quantum number S and the quantum number N associated with their combined rotational and electron-orbital angular momentum at low n values, to a situation where S and N mixing induced by the spin-rotation interaction in the ion core becomes observable. This analysis resulted in the insight that Rydberg extrapolation can be used to determine a pure rotational interval (i.e., without spin-rotation interaction), although, of course, the spin-rotation interval can, in principle, also be determined by extrapolation. The precision of our measurement was limited by the bandwidth of the radiation source used and the calibration procedure. The measurement procedure could be used to determine rotational intervals in other molecular ions which do not possess a permanent electric dipole moment and has the potential to be improved by using radiation sources with a narrower bandwidth, extending the measurement to higher n values and utilizing better frequency-calibration methods.

ACKNOWLEDGMENTS

We thank Dr. Daniel Sprecher for helpful discussions and his early contributions to this project. M.B. thanks the Laboratoire Aimé Cotton for the hospitality during an extended visit in 2013. This work is supported financially by the Swiss National Science Foundation under Project No. 200020-146759. Ch.J. was supported in part by the Ernst Miescher Foundation (Basel, Switzerland).

[1]L. Wolniewicz and J. D. Poll, Mol. Phys. **59**, 953 (1986).
[2]L. Wolniewicz and T. Orlikowski, Mol. Phys. **74**, 103 (1991).
[3]R. E. Moss, Mol. Phys. **80**, 1541 (1993).
[4]V. I. Korobov, Phys. Rev. A **74**, 052506 (2006).
[5]V. I. Korobov, Phys. Rev. A **77**, 022509 (2008).
[6]V. I. Korobov, L. Hilico, and J.-P. Karr, Phys. Rev. A **89**, 032511 (2014).
[7]D. M. Bishop, S.-K. Shih, C. L. Beckel, F.-M. Wu, and J. M. Peek, J. Chem. Phys. **63**, 4836 (1975).
[8]J. M. Taylor, Z.-C. Yan, A. Dalgarno, and J. F. Babb, Mol. Phys. **97**, 25 (1999).
[9]H. V. R. Vila, L. A. Leal, A. L. A. Fonseca, and R. Gargano, Int. J. Quantum Chem. **112**, 829 (2012).
[10]A. Carrington, I. R. McNab, and C. A. Montgomerie, Chem. Phys. Lett. **160**, 237 (1989).
[11]K. B. Jefferts, Phys. Rev. Lett. **20**, 39 (1968).
[12]K. B. Jefferts, Phys. Rev. Lett. **23**, 1476 (1969).
[13]G. Herzberg and Ch. Jungen, J. Mol. Spectrosc. **41**, 425 (1972).
[14]A. Osterwalder, A. Wüest, F. Merkt, and Ch. Jungen, J. Chem. Phys. **121**, 11810 (2004).
[15]Z. W. Fu, E. A. Hessels, and S. R. Lundeen, Phys. Rev. A **46**, R5313 (1992).
[16]P. W. Arcuni, E. A. Hessels, and S. R. Lundeen, Phys. Rev. A **41**, 3648 (1990).
[17]L. Åsbrink, Chem. Phys. Lett. **7**, 549 (1970).
[18]F. Merkt and T. P. Softley, J. Chem. Phys. **96**, 4149 (1992).
[19]C. Chang, C.-Y. Ng, S. Stimson, M. Evans, and C. W. Hsu, Chin. J. Chem. Phys. **20**, 352 (2007).
[20]J. Shen, A. Borodin, M. Hansen, and S. Schiller, Phys. Rev. A **85**, 032519 (2012).
[21]U. Bressel, A. Borodin, J. Shen, M. Hansen, I. Ernsting, and S. Schiller, Phys. Rev. Lett. **108**, 183003 (2012).
[22]D. Sprecher, Ch. Jungen, and F. Merkt, J. Chem. Phys. **140**, 104303 (2014).
[23]D. Sprecher, Ch. Jungen, W. Ubachs, and F. Merkt, Faraday Discuss. **150**, 51 (2011).
[24]J. Liu, H. Schmutz, and F. Merkt, J. Mol. Spectrosc. **256**, 111 (2009).
[25]Ch. Haase, J. A. Agner, and F. Merkt, J. Chem. Phys. **138**, 244202 (2013).
[26]A. Osterwalder and F. Merkt, Phys. Rev. Lett. **82**, 1831 (1999).
[27]U. Fano, Phys. Rev. A **2**, 353 (1970); erratum, *ibid.* **15**, 817 (1977).
[28]E. Fermi, Nuovo Cimento **11**, 157 (1934).
[29]Ch. Jungen, I. Dabrowski, G. Herzberg, and M. Vervloet, J. Chem. Phys. **93**, 2289 (1990).

25 July 2026 17:53:19